

Effects of ^{18}O isotopic substitution on the rotational spectra and potential splitting in the $\text{OH}-\text{OH}_2$ complex: Improved measurements for $^{16}\text{OH}-^{16}\text{OH}_2$ and $^{18}\text{OH}-^{18}\text{OH}_2$, new measurements for the mixed isotopic forms, and *ab initio* calculations of the ${}^2A'-{}^2A''$ energy separation

Carolyn S. Brauer,^{1,a)} Galen Sedo,¹ Erin Dahlke,^{1,b)} Shenghai Wu,¹ Erik M. Grumstrup,^{1,c)} Kenneth R. Leopold,^{1,d)} Mark D. Marshall,² Helen O. Leung,² and Donald G. Truhlar¹

¹Department of Chemistry, University of Minnesota, 207 Pleasant St., SE., Minneapolis, Minnesota 55455-0431, USA

²Department of Chemistry, Amherst College, P.O. Box 5000, Amherst, Massachusetts 01002-5000, USA

(Received 10 June 2008; accepted 28 July 2008; published online 9 September 2008)

Rotational spectra have been observed for $^{16}\text{OH}-^{16}\text{OH}_2$, $^{16}\text{OH}-^{18}\text{OH}_2$, $^{18}\text{OH}-^{16}\text{OH}_2$, and $^{18}\text{OH}-^{18}\text{OH}_2$ with complete resolution of the nuclear magnetic hyperfine structure from the OH and water protons. Transition frequencies have been analyzed for each isotopic form using the model of Marshall and Lester [J. Chem. Phys. **121**, 3019 (2004)], which accounts for partial quenching of the OH orbital angular momentum and the decoupling of the electronic spin from the OH molecular axis. The analysis accounts for both the ground (${}^2A'$) and first electronically excited (${}^2A''$) states of the system, which correspond roughly to occupancy by the odd electron in the p_y and p_x orbitals, respectively (where p_y is in the mirror plane of the complex and p_x is perpendicular to p_y and the OH bond axis). The spectroscopic measurements yield a parameter, ρ , which is equal to the vibrationally averaged ${}^2A'-{}^2A''$ energy separation that would be obtained if spin-orbit coupling and rotation were absent. For the parent species, $\rho = -146.560\,27(9)\text{ cm}^{-1}$. ^{18}O substitution on the water increases $|\rho|$ by $0.105\,29(10)\text{ cm}^{-1}$, while substitution on the OH decreases $|\rho|$ by $0.068\,64(11)\text{ cm}^{-1}$. In the $\text{OH}-\text{OH}_2$ complex, the observed value of ρ implies an energy spacing between the rotationless levels of the ${}^2A'$ and ${}^2A''$ states of 203.76 cm^{-1} . *Ab initio* calculations have been performed with quadratic configuration interaction with single and double excitations (QCISD), as well as multireference configuration interaction (MRCI), both with and without the inclusion of spin-orbit coupling. The MRCI calculations with spin-orbit coupling perform the best, giving a value of 171 cm^{-1} for the ${}^2A'-{}^2A''$ energy spacing at the equilibrium geometry. Calculations along the large-amplitude bending coordinates of the OH and OH_2 moieties within the complex are presented and are shown to be consistent with a vibrational averaging effect as the main cause of the observed isotopic sensitivity of ρ . © 2008 American Institute of Physics.
[DOI: 10.1063/1.2973638]

I. INTRODUCTION

The $\text{OH}-\text{OH}_2$ complex has been the subject of numerous investigations spanning well over a decade.^{1–17} Interest in this system stems from its fundamental role as a prototype for open-shell intermolecular interactions, from the importance of the OH radical in combustion, and from the recent recognition of the role of molecular complexes, especially water clusters, in atmospheric chemistry.^{18,19} The $\text{OH}-\text{OH}_2$ complex plays an important role in the reactions of OH with H_2O (Ref. 20) and atmospheric hydrocarbons;²¹ the former

role is analogous to that of the complex of OH with H_2S in the $\text{OH}+\text{H}_2\text{S}$ reaction.²² The $\text{OH}-\text{OH}_2$ complex also provides a starting point for understanding the hydration structures of OH in liquid water.^{23–25} Experimentally, $\text{OH}-\text{OH}_2$ has been observed by infrared spectroscopy in cryogenic matrices,^{4,6,7} and more recently by Fourier transform microwave spectroscopy in the gas phase.^{10,11} Theoretically, it has been studied by a variety of computational methods, which have focused on energetics, structure, and reactivity.^{1–3,5,6,8,12–17,20,21,23–25} Theory and experiment concur that the system is a hydrogen bonded complex with OH acting as the proton donor, and calculations suggest a small potential barrier at the planar configuration. This latter feature is similar to that in the closed-shell complex $\text{FH}-\text{OH}_2$, for which large-amplitude vibrational motion of the water subunit renders the complex effectively planar.²⁶

In a previous study, we reported microwave spectra of $^{16}\text{OH}-^{16}\text{OH}_2$ and $^{18}\text{OH}-^{18}\text{OH}_2$ and investigated the effects

^{a)}Present address: Jet Propulsion Laboratory, Pasadena, California 91109, USA.

^{b)}Present address: Department of Chemistry, Loras College, Dubuque, Iowa 52004-0178, USA.

^{c)}Present address: Department of Chemistry, University of Colorado, Boulder, Colorado 80309-0215, USA.

^{d)}Author to whom correspondence should be addressed. Electronic mail: kleopold@umn.edu.

of partially quenched electronic orbital angular momentum on its rotational spectrum and magnetic hyperfine interactions.¹⁰ Briefly, complexation with water breaks the cylindrical symmetry of free OH and quenches the orbital angular momentum by mixing states with well defined projections of this quantity onto the bond axis (i.e., by mixing the states corresponding to $\Lambda=+1$ and $\Lambda=-1$ states of free OH). The resulting electronic states of the complex, labeled ${}^2A'$ and ${}^2A''$ in its C_s equilibrium geometry, are separated in energy by an amount dependent on the spin-orbit coupling constant (which, to a good approximation may be assumed equal to that of free OH), on a spectroscopically determinable parameter, ρ , which describes the mixing,²⁷ and on the geometry of the complex. The electron spin angular momentum also decouples from the bond axis, and the decoupling of the spin and orbital angular momenta has a strong influence on the rotational spectrum of the system. Thus, the degree of quenching and the ${}^2A'-{}^2A''$ energy separation can be quantitatively assessed from the rotational spectrum of the complex. Although the rotational energy levels are only sensitive to the magnitude of ρ , the magnetic hyperfine structure depends on its sign, and from that dependence the ${}^2A'$ state was determined in our previous work to be the ground state of the system. The ${}^2A''$ state was estimated to lie ~ 200 cm^{-1} above the ground state.

The purpose of this paper is twofold. First, subsequent to the publication of Ref. 10, the presence of stray magnetic fields within our spectrometer was discovered. These fields caused shifts in recorded spectral frequencies by as much as several hundred kilohertz and, while their effects on our previously reported value of ρ were negligible, we wish to report here the improved spectral frequencies for the ${}^{16}\text{O}/{}^{16}\text{O}$ and ${}^{18}\text{O}/{}^{18}\text{O}$ isotopic forms. Second, although the fitted values of ρ differed by only 0.03% between the two isotopic forms studied, this difference was about 50 times the uncertainties estimated on the basis of our least-squares fits. Thus, in an effort to further examine this effect, we report new measurements for the ${}^{16}\text{OH}-{}^{18}\text{OH}_2$ and ${}^{18}\text{OH}-{}^{16}\text{OH}_2$ species. *Ab initio* calculations are also presented to explore the effect of distortion along the intermolecular degrees of freedom, and the observed isotopic dependence of ρ is shown to be consistent with changes due to vibrational averaging.

II. BACKGROUND

To facilitate comparison of the quantities that are measured and calculated in this work, a brief description of the spectroscopic model is presented here. This model was initially described in conjunction with infrared studies of OH–HCCH (Ref. 28) and later used to predict⁸ and analyze¹⁰ the microwave spectrum of OH–OH₂. Although a very complete presentation is given elsewhere,²⁷ a simplified discussion may be useful, particularly with regard to relating experimental and *ab initio* results.

The physical picture is as follows: in the ground state of free OH, the spin and orbital angular momenta, S and L , respectively, have constant projections of $\Sigma = \pm \frac{1}{2}$ and $\Lambda = \pm 1$ onto the OH bond axis. (All angular momenta are given in units of \hbar .) The electronic wave functions are

eigenfunctions of L_z and are designated $|\Lambda, \Sigma, \Omega\rangle$, where $\Omega = \Lambda + \Sigma$. States with $|\Omega| = \frac{3}{2}$ and $|\Omega| = \frac{1}{2}$ differ in energy due to the spin-orbit interaction. The spatial part of the electronic wave function depends on $e^{i\Lambda\phi}$ (where ϕ is the azimuthal angle specifying the coordinate of the unpaired electron) and gives rise to a cylindrically symmetric electron distribution since $(e^{i\Lambda\phi})^*(e^{i\Lambda\phi})$ is independent of ϕ . When OH forms a complex with water, however, the cylindrical symmetry is broken, and if the interaction were sufficiently strong, the electronic wave functions would be better described in terms of p_x and p_y orbitals on oxygen. These orbitals are 50:50 admixtures of $e^{+i\phi}$ and $e^{-i\phi}$ and are not eigenfunctions of L_z . In this situation, $\langle \psi_{\text{el}} | L_z | \psi_{\text{el}} \rangle = 0$ (where ψ_{el} is the electronic wave function), and the orbital angular momentum is said to be quenched. On the other hand, if the interaction with water were weak but still nonvanishing, the electronic wave functions may be best described as linear combinations of $\Lambda = +1$ and $\Lambda = -1$ states but not necessarily 50:50 admixtures. In this case, $0 < |\langle \psi_{\text{el}} | L_z | \psi_{\text{el}} \rangle| < 1$ and the orbital angular momentum is termed partially quenched. In the C_s symmetry of the equilibrium geometry of the complex, states corresponding to p_y and p_x are of ${}^2A'$ and ${}^2A''$ symmetry, respectively, where p_y is the orbital that lies in the bisector plane of the water, and p_x is the orbital that is perpendicular to both p_y and the OH bond axis.

Experimental spectra are analyzed using the Hamiltonian

$$\hat{H} = \hat{H}_{\text{rot}} + \hat{H}_{\text{SO}} + \hat{H}_q, \quad (1)$$

where \hat{H}_{rot} , \hat{H}_{SO} , and \hat{H}_q are the rotational, spin-orbit, and quenching Hamiltonians, respectively. \hat{H}_{rot} , which describes rotation of the nuclear frame, is rather lengthy and is given elsewhere.²⁷ \hat{H}_{SO} is approximated by

$$\hat{H}_{\text{SO}} = A_{\text{SO}} l_z s_z, \quad (2)$$

where A_{SO} is the vibrationally averaged spin-orbit constant of free OH, and lower case letters are used to represent the angular momentum operators in the complex. The projections of l and s onto the OH bond axis, assumed to be coincident with the vibrationally averaged a -axis of the complex, are designated λ and σ , respectively, with $\omega \equiv \lambda + \sigma$. In the next paragraph, we will further assume that the projection of the orbital angular momentum of the complex on z arises from that of free OH.

The term \hat{H}_q is given by^{27,29}

$$\hat{H}_q = \frac{\rho}{2} (\bar{l}_+^2 + \bar{l}_-^2), \quad (3)$$

where ρ is a vibrationally averaged parameter, and \bar{l}_{\pm} represents a normalized raising or lowering operator corresponding to the OH orbital angular momentum, viz., $\bar{l}_{\pm}^2 = l_{\pm}^2 / l(l+1)$. \hat{H}_q is empirically introduced into Eq. (1) as a simple means of describing the mixing between the $\lambda = +1$ and $\lambda = -1$ states of OH in the complex and, as such, it provides a measure of the degree of quenching of the orbital angular momentum. Note that the addition of this term to Eq. (1) defines the spectroscopic parameter ρ , which is to be determined from spectral data.

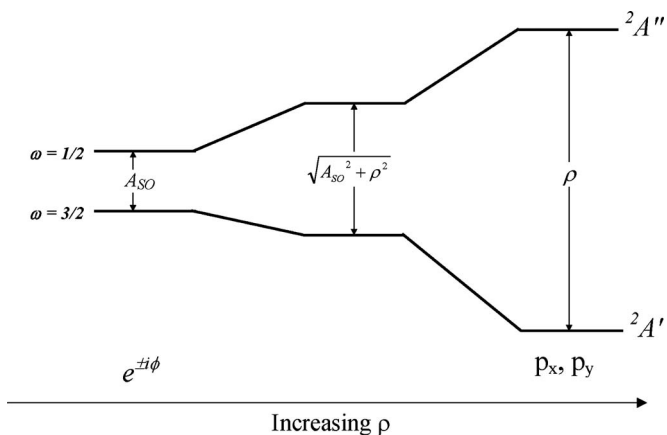


FIG. 1. An energy level diagram of an OH complex showing the effect of ρ on the ground and first excited state energy levels between $\rho=0$ (left) and $\rho \gg A_{SO}$ (right).

Matrix elements of \hat{H} have been given in Ref. 27. In the complete treatment, primitive basis functions $|J, p, M, \eta, \lambda, s, \sigma\rangle = |J, p, M\rangle |\eta, \lambda\rangle |s, \sigma\rangle$ are formed, where J is the total angular momentum quantum number exclusive of nuclear spin, p is its projection onto the a -inertial axis of the complex, and M is its projection onto a space-fixed axis. The symbol η is included to represent any additional quantum numbers needed to specify the electronic state. Since η and s are the same for all states considered in this work and since states of different M are degenerate in the absence of an external field, this basis may be abbreviated as $|J, p, \lambda, \sigma\rangle$. Although the full basis set is necessary to analyze the rotational spectrum of the complex, the meaning of ρ is most easily seen by examining the problem in the absence of rotation. If the rotational motion is ignored, the basis states are $|\eta, \lambda, s, \sigma\rangle$, abbreviated as $|\lambda, \sigma\rangle$, with matrix elements²⁷

$$\langle \lambda, \sigma | \hat{H}_{SO} | \lambda, \sigma \rangle = A_{SO} \lambda \sigma$$

and

$$\langle -\lambda, \sigma | \hat{H}_q | \lambda, \sigma \rangle = \rho / 2.$$

Thus, for each value of $\sigma = \pm 1/2$, $(\hat{H}_{SO} + \hat{H}_q)$ separates into a 2×2 block of the form

$$\begin{pmatrix} A_{SO}/2 & \rho/2 \\ \rho/2 & -A_{SO}/2 \end{pmatrix}$$

with eigenvalues $E = \pm \frac{1}{2} \sqrt{A_{SO}^2 + \rho^2}$. The ${}^2A' - {}^2A''$ energy separation, $\Delta E \equiv E({}^2A') - E({}^2A'')$ is thus given by $-\sqrt{A_{SO}^2 + \rho^2}$, where the minus sign arises because the ${}^2A'$ state is the ground state of the system. A schematic diagram is shown in Fig. 1.

It is apparent from Fig. 1 that when $\rho \ll A_{SO}$, the electronic states of the complex are best described using the $\omega = \frac{3}{2}$ and $\omega = \frac{1}{2}$ states of OH, with wave functions $e^{i\Lambda\phi}$ and an energy separation of A_{SO} . In the opposite limit, when $\rho \gg A_{SO}$, the electronic wave function is the molecular orbital corresponding to either the p_x or p_y orbital, with energy separation in the absence of rotation equal to ρ . OH–OH₂ lies in the intermediate regime, in which $\rho \approx A_{SO}$, and thus both ρ and A_{SO} contribute to the energy separation between elec-

tronic states. Note that the spin-orbit interaction mixes the ${}^2A'$ and ${}^2A''$ electronic states, and that ρ is the ${}^2A' - {}^2A''$ energy separation that would be obtained if the spin-orbit interaction and rotation were absent.

The full basis set, including rotation, is a parity conserving basis $|J, P, \lambda, \sigma, \varepsilon\rangle$, formed from linear combination of the primitive functions $|J, p, \lambda, \sigma\rangle$, viz.,

$$|J, P, \lambda, \sigma, \varepsilon\rangle = (1/2)^{1/2} \{ |J, P, \lambda, \sigma\rangle + \varepsilon (-1)^{(J-1/2)} |J, -P, -\lambda, -\sigma\rangle \}, \quad (4)$$

where $P = |p|$, and $\varepsilon = \pm 1$ designates the parity of the state. Note that although the symmetry of the electronic wave functions has been designated in the C_s symmetry of the equilibrium structure of the complex (i.e., by ${}^2A'$ and ${}^2A''$), the functions given in Eq. (4) are eigenfunctions of parity in the vibrationally averaged structure of the complex, which is presumed to be C_{2v} .

In this paper, we examine the variation in the spectroscopically determined values of ρ with isotopic substitution on both the OH and OH₂ moieties. As noted above, ρ is a vibrationally averaged parameter, which describes the electronic state energy changes arising from the loss of cylindrical symmetry of the OH upon complexation. *Ab initio* electronic structure calculations are used to explore these changes as a function of large-amplitude vibrational motions and the observed isotopic dependence of ρ is shown to be consistent, both in sign and magnitude, with the expected changes arising from differences in vibrationally averaged structure.

III. EXPERIMENTAL METHODS AND RESULTS

Spectra were recorded using a pulsed-nozzle Fourier transform microwave spectrometer in operation at the University of Minnesota since the early 1990s.³⁰ The discovery that prompted this work was our recognition that our spectral frequencies for ${}^{16}\text{OH} - {}^{16}\text{OH}_2$ disagreed, in some cases by several hundred kilohertz, with those measured elsewhere.³¹ The problem was traced to the 440 stainless steel that had been originally used to construct the support rods for the spectrometer's mirror assembly. These introduced significant inhomogeneous magnetic fields that could not be nullified by the existing Helmholtz coils and produced the spectral shifts observed. The conversion to 316 stainless steel rods immediately eliminated these fields and led to the new frequencies reported below.³²

It is perhaps a worthwhile cautionary note that prior to the conversion to 316 stainless steel, literature spectra of four different open-shell molecules were recorded on the spectrometer with line widths less than 25 kHz and line centers within 6 kHz of the literature values. These transitions were the following: ${}^{16}\text{OH}$ (Ref. 33): $(J, F, \Omega) = (\frac{1}{2}, 1, \frac{1}{2}) \leftarrow (\frac{1}{2}, 1, \frac{1}{2})$ and $(J, F, \Omega) = (\frac{5}{2}, 2, \frac{3}{2}) \leftarrow (\frac{5}{2}, 2, \frac{3}{2})$ (lambda doubling transitions); Ar– ${}^{16}\text{OH}$ (Ref. 34): $(J, F) = (\frac{5}{2}, 3) \leftarrow (\frac{3}{2}, 2)$; ${}^{56}\text{FeCO}$ (Ref. 35): $(J=1 \leftarrow 0; J=2 \leftarrow 1)$; Ar– ${}^{32}\text{SH}$ (Ref. 36): $(J, F) = (\frac{7}{2}, 3) \leftarrow (\frac{5}{2}, 2)$. (F is the total angular momentum quantum number including nuclear spin.) Thus, the OH–OH₂ spectra appear, at least in some respect, to exhibit a greater sensitivity to stray fields than those of other, ostensibly similar para-

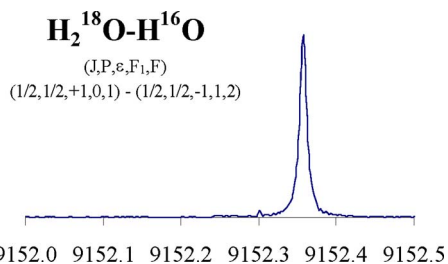


FIG. 2. (Color online) A single hyperfine component in the spectrum of $^{16}\text{OH}-^{18}\text{OH}_2$. Frequency values are in MHz. This spectrum represents the average of 500 gas pulses with six free induction decay signals recorded per pulse.

magnetic species. Although initially surprising, a simple explanation for this observation may lie, in part, in a second order Zeeman effect between $M_F=0$ states that are in unusually close proximity to due to the water superhyperfine structure.^{10,11} (M_F is the projection of F onto a space-fixed axis.) Ordinarily, since the first order Zeeman effect is proportional to M_F , the $M_F=0 \leftarrow 0$ components can persist at the zero-field frequency in the presence of a nonzero magnetic field, and it is likely that this was the component observed in each of the test systems studied. In $\text{OH}-\text{H}_2\text{O}$, however, the superhyperfine structure produces very closely spaced states of the same M_F , which couple within the same M_F block of the Hamiltonian.^{10,11} Thus, each M_F level may be perturbed

by the second order Zeeman effect and even the $M_F=0 \leftarrow 0$ transitions, therefore, lose their immunity from Zeeman tuning. As a result, no transitions occur at the zero-field frequency in the presence of an external field. Calculations support the plausibility of such a scenario³⁷ but also indicate that both $M_F=0 \leftarrow 0$ and $M_F=1 \leftarrow 1$ transitions may have been recorded in our previous study.

The $\text{OH}-\text{H}_2\text{O}$ complex was produced as in our previous work by bubbling Ar through water and expanding through a pulsed nozzle fitted with a dc discharge assembly. For observation of the mixed isotopic forms, a mixture of H_2^{16}O and H_2^{18}O was used. Optimum signals were obtained with a backing pressure of Ar equal to about 2.7 atm, and the nozzle repetition rate was set at 5 s^{-1} . Transition frequencies are typically accurate to about 20 kHz. A representative spectrum is shown in Fig. 2. Spectral frequencies and assignments corresponding to the four isotopically substituted forms of $\text{OH}-\text{OH}_2$ observed are listed in Table I.

Nuclear hyperfine structure was treated with the coupling scheme $F_1 = J + I$, $F = F_1 + I_w$, where I and I_w refer to the proton nuclear spins of the OH and H_2O , respectively, and the magnetic hyperfine Hamiltonian was taken from Howard and co-workers.^{38,39} Because the protons are fermions, states observed in this work are required to have $I_w = 1$.²⁷ For each rotational transition observed, the hyperfine structure appears as a set of widely spaced components arising

TABLE I. Observed microwave transitions of $\text{OH}-\text{OH}_2$.

$F'_{F_1'} \leftarrow F''_{F_1''}$	Frequency ^a (MHz)			
	$^{16}\text{OH}-^{16}\text{OH}_2$	$^{18}\text{OH}-^{18}\text{OH}_2$ $(J, P, \epsilon) = (\frac{1}{2}, \frac{1}{2}, -1) \leftarrow (\frac{1}{2}, \frac{1}{2}, +1)$	$^{16}\text{OH}-^{18}\text{OH}_2$	$^{18}\text{OH}-^{16}\text{OH}_2$
$1_0 \leftarrow 2_1$	9484.334(0.003)	8530.399(0.001)	9072.065(0.000)	8944.392(0.003)
$1_0 \leftarrow 1_1$	9485.314(-0.008)	8531.375(-0.006)	9073.044(-0.004)	8945.371(-0.006)
$1_0 \leftarrow 0_1$	9485.736(-0.005)	8531.794(-0.003)	9073.466(0.001)	8945.793(-0.001)
$0_1 \leftarrow 1_0$	9560.672(-0.004)	8606.788(-0.002)	9148.376(-0.003)	9020.801(0.003)
$1_1 \leftarrow 1_0$	9562.038(-0.007)	8608.157(0.000)	9149.747(0.000)	9022.167(0.001)
$2_1 \leftarrow 1_0$	9564.651(-0.009)	8610.766(-0.001)	9152.358(-0.001)	9024.783(0.004)
$0_1 \leftarrow 1_1$	9569.527(0.006)	8615.690(0.003)	9157.288(0.000)	9029.640(-0.002)
$1_1 \leftarrow 2_1$	9569.909(0.008)	8616.074(0.003)	9157.678(0.005)	9030.023(0.000)
$1_1 \leftarrow 1_1$	9570.893(0.002)	8617.048(-0.006)	9158.659(0.003)	9031.013(0.003)
$1_1 \leftarrow 0_1$	9571.316(0.006)	8617.472(0.002)	9159.075(0.002)	9031.427(0.000)
$2_1 \leftarrow 2_1$	9572.523(0.008)	8618.682(0.001)	9160.285(0.000)	9032.632(-0.004)
$2_1 \leftarrow 1_1$	9573.506(0.000)	8619.669(0.005)	9161.265(-0.003)	9033.622(-0.001)
		$(J, P, \epsilon) = (\frac{3}{2}, \frac{1}{2}, -1) \leftarrow (\frac{1}{2}, \frac{1}{2}, +1)$		
$3_2 \leftarrow 2_1$	14 951.418(0.008)	13 455.614(0.006)	14 299.553(0.000)	14 110.251(0.002)
$2_2 \leftarrow 1_1$	14 952.390(0.024)	13 456.584(0.025)	14 300.520(0.015)	14 111.220(0.017)
$1_2 \leftarrow 0_1$	14 952.779(0.018)	13 456.961(0.008)	14 300.902(0.002)	14 111.602(0.004)
$0_1 \leftarrow 1_0$	14 965.926(0.002)	13 470.109(-0.008)	14 314.048(-0.001)	14 124.766(-0.008)
$1_1 \leftarrow 1_0$	14 965.946(-0.001)	13 470.135(-0.003)	14 314.072(0.002)	14 124.792(-0.004)
$2_1 \leftarrow 1_0$	14 965.981(-0.010)	13 470.170(-0.010)	14 314.102(-0.008)	14 124.831(-0.009)
$1_1 \leftarrow 2_1$	14 973.802(0.000)	13 478.064(0.011)	14 322.001(0.005)	14 132.662(0.008)
$2_1 \leftarrow 2_1$	14 973.830(-0.017)	13 478.095(0.001)	14 322.025(-0.012)	14 132.687(-0.010)
$0_1 \leftarrow 1_1$	14 974.757(-0.013)	13 478.995(-0.019)	14 322.951(-0.007)	14 133.619(0.000)
$1_1 \leftarrow 1_1$	14 974.792(-0.001)	13 479.025(-0.010)	14 322.985(0.006)	14 133.648(0.007)
$2_1 \leftarrow 1_1$	14 974.826(-0.011)	13 479.068(-0.009)	...	14 133.684(0.000)
$1_1 \leftarrow 0_1$	14 975.214(0.003)	13 479.459(0.008)	14 323.393(-0.002)	14 134.052(-0.006)
rms (MHz)	0.010	0.009	0.005	0.006

^aNumbers in parentheses represent residuals from the least-squares fit. All transitions correspond to $\omega = +\frac{3}{2}$. Root mean squared (rms) residual in the least-squares fit is in MHz.

TABLE II. Spectroscopic constants for isotopic forms of OH–OH₂.

	¹⁶ OH– ¹⁶ OH ₂	¹⁸ OH– ¹⁸ OH ₂	¹⁶ OH– ¹⁸ OH ₂	¹⁸ OH– ¹⁶ OH ₂
	Fitted parameters ^a			
(B+C)/2	6580.7444(11)	5922.5217(10)	6294.45760(62)	6210.00801(67)
ρ[cm ⁻¹]	-146.560 27(9)	-146.600 84(9)	-146.665 56(5)	-146.491 63(6)
b _F (OH)	-60.4176(70)	-60.5368(64)	-60.4852(39)	-60.4852(43)
b _F (H ₂ O)	-0.5182(47)	-0.5228(43)	-0.5228(28)	-0.5208(29)
x	-0.130 516(64)	-0.129 636(60)	-0.130 242(36)	-0.129 939(40)
y	0.028 867(56)	0.028 808(52)	0.028 829(32)	0.028 838(35)
	Fixed parameters ^b			
A	288 044.1	288 044.1	288 044.1	288 044.1
A _{SO}	-4 168 639.13	-4 168 644.9	-4 168 639.13	-4 168 644.9
(B–C)/2	50.	50.	50.	50.
a _{OH}	86.1118	86.1248	86.1118	86.1248
c _{OH}	130.2212	130.220	130.2212	130.220
d _{OH}	56.655	56.6664	56.655	56.6664

^aValues are in MHz, except as noted. Numbers in parentheses are one standard error in the least-squares fits.

^bThe spin–orbit constants for free ¹⁶OH and ¹⁸OH are taken from Refs. 40 and 41, respectively. OH hyperfine constants are from Ref. 42. The observed spectra are insensitive to the choice of A and (B–C)/2. See Ref. 10.

from the OH proton spin (and corresponding to different values of F_1), with each component further split into a closely spaced set of superhyperfine components differing in their values of F . For the ¹⁶OH–¹⁶OH₂ and ¹⁸OH–¹⁸OH₂ isotopic forms, the F_1 assignments are unchanged relative to those in our previous work, and only a few of the F assignments have been revised.

The observed transitions are sensitive to combinations of the nuclear hyperfine coupling constants, but the data are not sufficient for their independent determination. Thus, the same approximation used in our previous work¹⁰ was made, namely, that the spin-dipolar constants for the OH moiety in the complex, a , c , and d , change by a uniform percentage upon complexation, viz.,

$$a_{\text{complex}} = a_{\text{OH}}(1 + x), \quad (5)$$

$$c_{\text{complex}} = c_{\text{OH}}(1 + x), \quad (6)$$

and

$$d_{\text{complex}} = d_{\text{OH}}(1 + x). \quad (7)$$

This idea arises from the observation³⁹ that a , c , and d for a given nucleus all depend, to a first approximation, on $\langle 1/r^3 \rangle$, where r is the distance between the odd electron and the nucleus. The constraints imposed by Eqs. (5)–(7) allow the hyperfine structure to be analyzed using only two parameters for the OH: x and b_F (the Fermi contact parameter). In our previous paper, the superhyperfine structure arising from the water protons was treated by including only a Fermi contact term, $b_F(\text{H}_2\text{O})$, but the new measurements reported here indicated that an approach similar to that in Eqs. (5)–(7) is needed. In this case, $a(\text{H}_2\text{O})$, $c(\text{H}_2\text{O})$, and $d(\text{H}_2\text{O})$ were all scaled from the free-OH proton parameters as follows:

$$a(\text{H}_2\text{O}) = ya_{\text{OH}}, \quad (8)$$

$$c(\text{H}_2\text{O}) = yc_{\text{OH}}, \quad (9)$$

and

$$d(\text{H}_2\text{O}) = yd_{\text{OH}}. \quad (10)$$

Fitted values of the spectroscopic constants are given in Table II, together with a summary of constants constrained in the fits. Spectra were fit with rms residuals of typically 5–10 kHz, and the most important constants for ¹⁶OH–¹⁶OH₂ and ¹⁸OH–¹⁸OH₂, namely, ρ and (B+C)/2, are very similar to those given in our previous work.¹⁰ Values of (B+C)/2, for example, differ by less than 70 kHz, and the quenching parameter, ρ , differs by about 0.34 cm⁻¹. For the latter, much of this change arises not from the new data but from improved values of the spin-orbit constants of ¹⁶OH and ¹⁸OH used in the fits.⁴³

A few comments about the nuclear hyperfine parameters are appropriate. In an initial series of spectral fits utilizing the program applied in our previous work, very similar hyperfine parameters were obtained to those previously reported. However, despite the improved data, the rms residuals were curiously large (nearly 30 kHz) with some transitions showing residuals of as large as 80 kHz. Our original work utilized the hyperfine matrix elements of Mills *et al.*³⁸ but we have since rederived these matrix elements and have discovered small differences, even after properly accounting for the redefinition of angle used to specify the relative orientation of the OH axis and the a -axis of the complex. These new matrix elements, which are in agreement with those of Dennis *et al.*,³⁹ were used successfully in a recent publication⁴⁴ to fit the spectra of O₂–HF and O₂–DF, and their incorporation into the present work immediately reduced the rms residuals to the 5–10 kHz range noted above. With the new matrix elements, however, the values of x and b_F are rather different from those previously reported. For example, the value of x changes from 0.33 to -0.13, while b_F is reduced in magnitude from -155 to -60 MHz. Although these changes are significant, it remains the case that the fitted OH hyperfine parameters of the complex are quite different from those of free OH.

We also note that the magnetic hyperfine constants reported here are significantly different from those of Ohshima

*et al.*¹¹ Specifically, while we obtain $b_F = -60.4$ MHz and $c = c_{\text{OH}}(1+x) = 113.2$ MHz for the parent form, Ohshima *et al.*¹¹ reported $b_F = -8.23$ MHz and $T_{aa} = 2c/3 = 126.16$ MHz, the latter giving $c = 189.2$ MHz. While these results are perhaps initially surprising, significant differences between the two sets of constants can be expected for two reasons. First, and most obvious, is that different sets of hyperfine constants were used to fit the spectra in the two studies. In particular, in our work, the electronic orbital–nuclear spin coupling constant a was scaled according to Eq. (5) but nonetheless included in the analysis. In the work of Ohshima *et al.*,¹¹ however, a was excluded (i.e., effectively set to zero). Since the hyperfine structure depends on combinations of the hyperfine constants, constraints placed on one parameter necessarily affect the fitted values of the others. A second and perhaps less obvious reason lies in the different models used to describe the system. In our work, spectra were analyzed using a two-state model, which simultaneously accounts for the ${}^2A'$ and ${}^2A''$ electronic states and allows for partial quenching of the electronic orbital angular momentum in the complex. The analysis of Ohshima *et al.*,¹¹ on the other hand, considered a single electronic state in which the orbital angular momentum is fully quenched and used the spin-rotation coupling constants to approximate all the interactions between the two low-lying electronic states. Thus, couplings between the ground and low-lying excited electronic states were treated differently and this, too, affects the reported hyperfine parameters. While both treatments successfully reproduce the spectral data, we prefer the two-state model and the inclusion of the a constant to reflect the incomplete quenching of the orbital angular momentum. It should be emphasized, however, that *both* treatments employ their own approximations and both sets of constants, therefore, are probably best regarded as effective constants.

Careful examination of the energy levels obtained from the fitted spectroscopic constants allows a more accurate determination of the energy difference between the ground (${}^2A'$) and first excited (${}^2A''$) states of the system to be made. The lowest rotational level in ${}^2A'$ state is the (very slightly) parity doubled $|J, P, \omega\rangle = |\frac{3}{2}, \frac{3}{2}, \frac{3}{2}\rangle$ level at 0.0000 and 0.0001 cm^{-1} . Correspondingly, the lowest rotational level in ${}^2A''$ state is the (somewhat more) parity doubled $|J, P, \omega\rangle = |\frac{1}{2}, \frac{1}{2}, \frac{1}{2}\rangle$ level at 203.7555 and 203.7569 cm^{-1} . (These states are 81% p_y character and 9% p_x character, respectively.) The value of ΔE , therefore, as given by experiment in conjunction with the current model, is -203.76 cm^{-1} . Here, the two decimal place accuracy is appropriate to the energy separation either between the centers of the parity doublets or between their lower components. A direct measurement of this energy separation, perhaps by infrared combination differences, would provide a very stringent test of the spectroscopic model employed.

Finally, in view of the rather different treatments employed in this work and that of Ohshima *et al.*,¹¹ we decided to refit our own data for the parent species using the more conventional spin-rotation formalism. Using Pickett's SPFIT,⁴⁵ fitted values of $(B+C)/2$, Δ_N , $(\epsilon_{bb} + \epsilon_{cc})/2$, and the nuclear hyperfine parameters all agree with those reported in Ref. 11 to within the estimated uncertainties (where Δ_N is the

quartic centrifugal distortion constant and ϵ_{bb} and ϵ_{cc} are components of the spin-rotation tensor). In our fits, we found unit correlation between $(\epsilon_{bb} + \epsilon_{cc})/2$ and $(\epsilon_{bb} - \epsilon_{cc})$ and thus fixed the latter at the value reported in Ref. 11. Using just the Fermi contact and spin-dipolar magnetic hyperfine parameters, a rms residual of 17 kHz was obtained, although we found that this value could be reduced to about 6 kHz by inclusion of a distortion term in the OH Fermi contact constant. Although a simple approximate relationship between ϵ_{aa} and ρ has been deduced for the fully quenched limit,²⁷ given the complex manner in which quenching parameter and the spin-rotation constants affect the rotational energies of the complex, a simple analytical expression relating ρ and $(\epsilon_{bb} + \epsilon_{cc})/2$ does not seem obvious. However, Ohshima *et al.*¹¹ have argued that their observed spin-rotation doubling implies a ${}^2A' - {}^2A''$ energy separation of ~ 150 cm^{-1} , which is in very good agreement with the 146.56 cm^{-1} value given in Table II. Thus, in this sense, Ohshima *et al.* have already established reasonable consistency between the two treatments.⁴⁶

IV. ELECTRONIC STRUCTURE METHODS AND RESULTS

In light of the isotopic dependence of ρ noted in Sec. I, electronic structure computations were carried out to explore the variations in the ${}^2A' - {}^2A''$ energy separation as the complex is distorted along its intermolecular vibrational coordinates. The OH–H₂O complex was optimized in C_s symmetry for the ${}^2A'$ and ${}^2A''$ electronic states and in C_{2v} symmetry for the same two electronic states, which are now planar 2B_1 and 2B_2 electronic states, respectively. These calculations were carried out with quadratic configuration interaction with single and double excitations⁴⁷ (QCISD) with the 6–311+G(2df,2p) basis set^{48–50} by using the GAUSSIAN 03 software package.⁵¹ Spin-orbit coupling is neglected in all the QCISD calculations. The optimized structures, shown in Fig. 3, are consistent with those from previous calculations.^{2,3,6} Harmonic frequency analysis verified that the ${}^2A'$ and ${}^2A''$ states are local minima, while the 2B_1 and 2B_2 states are first order saddle points corresponding to transition states for degenerate inversion of the nonplanar states.

Table III compares the present QCISD/6–311+G(2df,2p) binding energies for the two electronic states, each at the planar and nonplanar optimized geometries, with those from previous work. All five methods represented in the table predict the ${}^2A'$ state to be 110–130 cm^{-1} lower in energy than the ${}^2A''$ state. The present work shows that there is a small barrier of ~ 15 cm^{-1} for inversion between the two minima, which is consistent with similar results of Xie *et al.*²

Previous studies of the excited electronic states of OH radical and the OH–H₂O complex⁸ have utilized the complete active space self-consistent field (CASSCF) method and multireference configuration interaction (MRCI) including single and double excitations,^{52,53} where the MRCI calculations use the same active space and are based on the state-averaged CASSCF molecular orbitals.⁵⁴ We have adopted the same approach here for calculating the splitting between the ${}^2A'$ and ${}^2A''$ states and have also calculated the

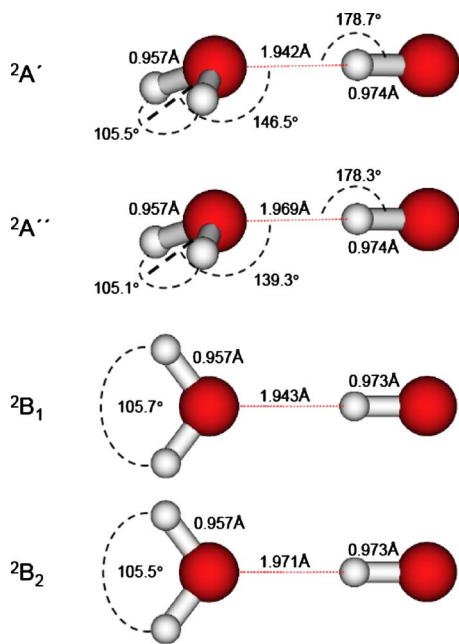


FIG. 3. (Color online) QCISD/6-311+G(2df,2p) optimized geometry for $^2A'$ (ground), $^2A''$, 2B_1 , and 2B_2 states.

spin-orbit coupling between the two states using the Breit-Pauli operator⁵⁵ (also using the same active space). The calculation including spin-orbit coupling will be called MRCI+SO. All multireference and spin-orbit calculations were carried out using the MOLPRO 2002.6 program⁵⁶ and are based on the fully decontracted aug-cc-pVTZ basis set on oxygen and the fully decontracted cc-pVTZ basis set on hydrogen. (Decontraction is necessary for the spin-orbit calculation in MOLPRO 2002.6.) In all CASSCF calculations, a full valence active space was used (15 electrons in 11 active orbitals), and the 1s orbitals of both oxygen atoms were doubly occupied and frozen at the restricted open-shell Hartree-Fock⁵⁷ level of theory.

Using the $^2A'$ optimized geometry, the $^2A'-^2A''$ energy separation $\Delta E \equiv E(^2A') - E(^2A'')$ was calculated to be -103.4 and -107.5 cm^{-1} at the CASSCF and MRCI levels of theory, respectively. Inclusion of the spin-orbit effects increases the splitting to -170.9 cm^{-1} . These results are consistent with the results from previous work,^{2,3,6} which have ranged from -110 to -190 cm^{-1} . As noted above, the value of ΔE derived from the analysis of microwave data is -203.76 cm^{-1} .

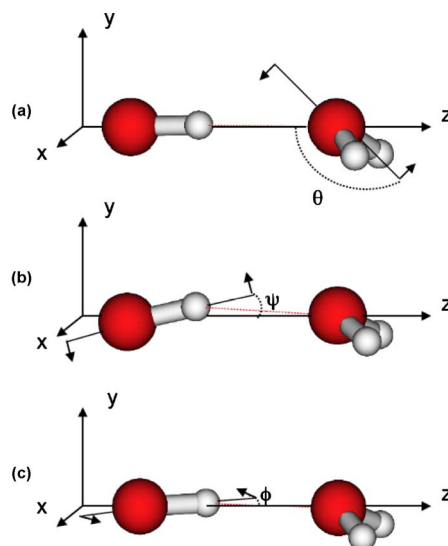


FIG. 4. (Color online) Diagram of internal motions considered. The rotations shown are about the monomers' centers of mass. (a) Rotation of H₂O about an axis parallel to the x -axis. Counterclockwise rotation corresponds to an increasing value of θ . (b) In-plane rotation of OH about an axis parallel to the x -axis. (c) Out-of-plane rotation of OH about an axis parallel to the y -axis.

V. EFFECT OF VIBRATIONAL DISTORTION ON ΔE

The OH–H₂O complex will be described with the y - z plane as the mirror plane and the z -axis connecting the centers of mass of the two monomers (see Fig. 4). In order to examine the effect of vibrational motion on the value of ΔE , three different internal rotations of the monomers about their centers of mass were considered: an internal rotation of the H₂O about an axis parallel to the x -axis, denoted by θ [see Fig. 4(a)], an internal rotation of the hydroxyl radical about an axis parallel to the x -axis, denoted by ψ [i.e., an internal rotation of the OH in the yz plane, see Fig. 4(b)], and an internal rotation of the hydroxyl radical about an axis parallel to the y -axis, denoted by ϕ [i.e., an internal rotation of the OH out of the yz plane, see Fig. 4(c)]. For the water unit, rotation about an axis parallel to the x axis describes the motion along the inversion coordinate in the complex and corresponds to the rotation about its axis of least moment of inertia (the a -axis). The perpendicular motion (i.e., an internal rotation about an axis parallel to the y -axis) was not considered, as this vibration is likely much stiffer (by anal-

TABLE III. Comparison of binding energies (cm^{-1}) for the two electronic states calculated without spin-orbit coupling.

		D_e^a				
Geometry	State	QCISD/ 6-311+G(2df,2p) ^b	RCISD/TZ2P ^c	UMP2/ 6-311+G(2d,2p) ^d	CCSD(T)/ 6-311+G(2d,2p) ^d	CCISD/ 6-311+G(2d,2p) ^e
Nonplanar	$^2A'$	-2008	-1969	-2078	-2053	-1990
	$^2A''$	-1897	-1857	-1962	-1941	-1878
Planar	2B_1	-1992	-1955			
	2B_2	-1858	-1829			

^a $D_e = E_{\text{OH-H}_2\text{O}} - E_{\text{OH}} - E_{\text{H}_2\text{O}}$.

^bPresent work.

^cReference 2.

^dReference 3.

^eReference 6.

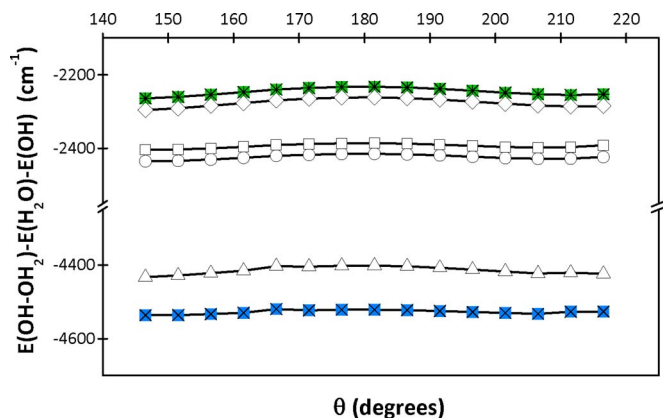


FIG. 5. (Color online) Plot of $E(\text{OH}-\text{OH}_2)-E(\text{H}_2\text{O})-E(\text{OH})$ (in cm^{-1}) vs θ for rotation of H_2O about an axis parallel to the x -axis and through its center of mass. $E(\text{OH})$ corresponds to the $\Omega=3/2$ state of the hydroxyl radical. Asterisks and circles indicate the MRCI+SO $^2A''$ and $^2A'$ energies, respectively, diamonds and squares indicate the MRCI $^2A''$ and $^2A'$ energies, respectively, and triangles and crosses indicate the CASSCF $^2A''$ and $^2A'$ energies, respectively.

ogy with $\text{FH}-\text{OH}_2$ ^{26(b),58} and, moreover, corresponds to the rotation of water about its axis of largest moment of inertia (the c -axis) when the complex is in its vibrationally averaged planar configuration. Since the moment of inertia acts roughly as the reduced mass for the bending vibration,⁵⁹ a large moment of inertia will act in concert with the larger force constant to attenuate the amplitude of the perpendicular vibration. For the OH moiety, however, both in-plane and out-of-plane motions were considered, as these vibrations correspond to rotation of the diatom about the axes of equal moment of inertia and are therefore expected to be comparable in their amplitudes (assuming the force constants are not widely disparate). For each internal rotation, the monomer units were frozen in the geometry of the global-minimum-energy complex and rotated around the axis of interest in 5° increments for the H_2O rotation and the out-of-plane OH rotation and increments of 10° for the OH in-plane rotation.

Figures 5–7 show the energies of association of the complex, $E(\text{OH}-\text{OH}_2)-E(\text{H}_2\text{O})-E(\text{OH})$, as a function of θ , ψ , and ϕ , respectively, calculated using the CASSCF and MRCI methods. Binding energies for the MRCI+SO calculations are also given as a function of θ and ψ in Figs. 5 and 6. Here, $E(\text{OH}-\text{OH}_2)$ is the energy of either the $^2A'$ or $^2A''$ state of $\text{OH}-\text{OH}_2$, $E(\text{H}_2\text{O})$ is the ground state energy of water, and $E(\text{OH})$ is the energy of the lowest ($\Omega=3/2$) state of free OH. Clearly, the energies of the $^2A'$ and $^2A''$ states vary only slightly with the angle describing the water inversion (θ) but are considerably more sensitive to changes along the coordinates describing the OH orientation (ψ and ϕ). Since we are mainly concerned in this work with the energy difference between the $^2A'$ and $^2A''$ states, values of $\Delta E=E(^2A')-E(^2A'')$ are plotted versus θ , ψ , and ϕ in Figs. 8–10, respectively. These results are discussed in more detail below.

It is apparent from Fig. 8 that the magnitude of ΔE increases as θ moves away from the equilibrium angle of 146.5° , reaching an estimated maximum value at ΔE equal to -119.5 , -124.3 , and -182.0 cm^{-1} for the CASSCF, MRCI,

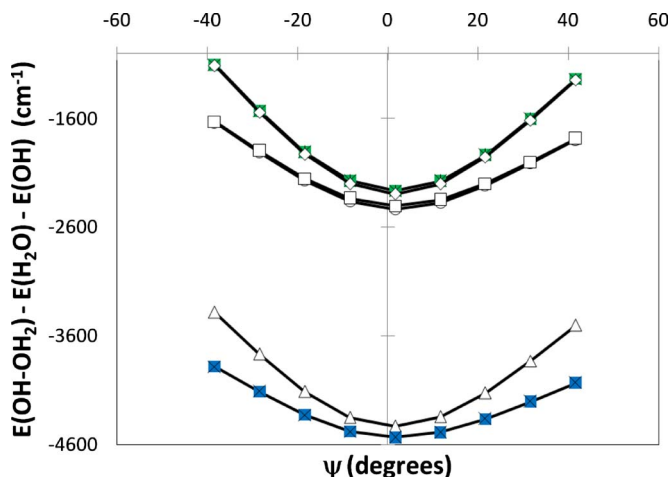


FIG. 6. (Color online) Plot of $E(\text{OH}-\text{OH}_2)-E(\text{H}_2\text{O})-E(\text{OH})$ (in cm^{-1}) vs ψ for rotation of OH radical about an axis parallel to the x -axis and through the center of mass of OH (in-plane rotation through angle ψ). $E(\text{OH})$ corresponds to the $\Omega=3/2$ state of the hydroxyl radical. Asterisks and circles indicate the MRCI+SO $^2A''$ and $^2A'$ energies, respectively, diamonds and squares indicate the MRCI $^2A''$ and $^2A'$ energies, respectively, and triangles and crosses indicate the CASSCF $^2A''$ and $^2A'$ energies, respectively. Note that the MRCI+SO energies are partially obscured by the MRCI energies.

and MRCI+SO calculations, respectively, at the planar geometry (corresponding to the 2B_1 - 2B_2 splitting). This indicates increases in the magnitude of the splitting of 16.1, 16.8, and 11.1 cm^{-1} for the CASSCF, MRCI, and MRCI+SO methods, respectively, as one goes from the equilibrium structure to the planar saddle point geometry. These numbers are consistent with the value obtained from the QCISD/6-311+G(2df,2p) optimizations described above, which gave a 2B_1 - 2B_2 splitting of -134 cm^{-1} . Examining how rapidly the value of ΔE changes with respect to θ shows that for geometries close to the global minimum structure, the magnitude of the derivative of ΔE with respect to θ is approximately 0.8 $\text{cm}^{-1}/\text{deg}$ for the CASSCF and MRCI method, and about 0.6 $\text{cm}^{-1}/\text{deg}$ for the full MRCI+SO method. In general, we see that the CASSCF and MRCI

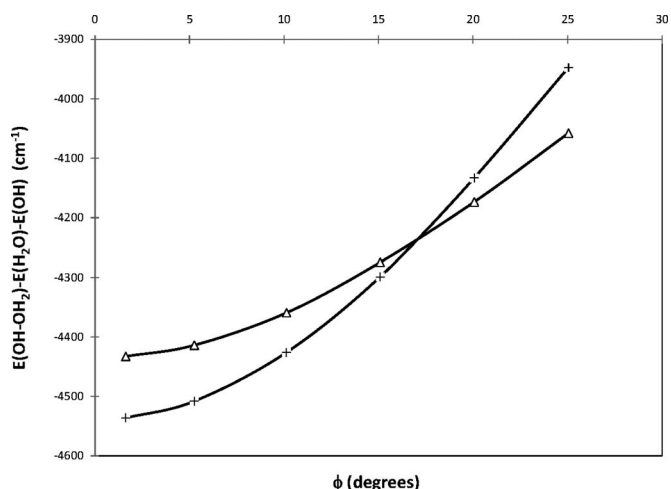


FIG. 7. Plot of $E(\text{OH}-\text{OH}_2)-E(\text{H}_2\text{O})-E(\text{OH})$ (in cm^{-1}) vs ϕ for rotation of OH radical about an axis parallel to the y -axis and through its center of mass (out-of-plane rotation). Triangles and crosses indicate the CASSCF $^2A''$ and $^2A'$ states, respectively.

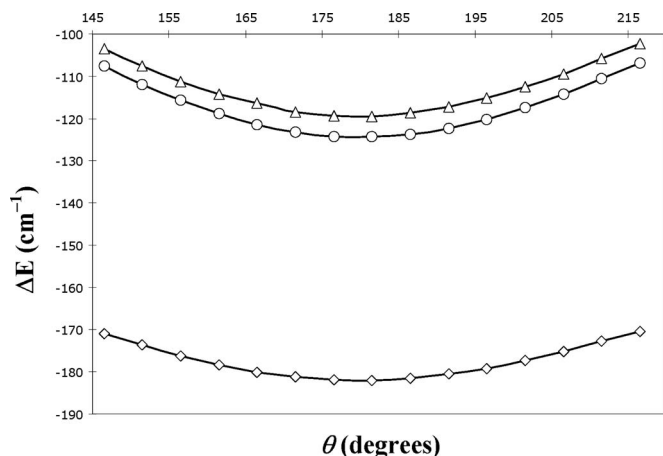


FIG. 8. Plot of $\Delta E \equiv E(^2A') - E(^2A'')$ (in cm^{-1}) vs θ for rotation of H_2O about an axis parallel to the x -axis and through its center of mass. Triangles, circles, and diamonds indicate results obtained using the CASSCF, MRCI, and MRCI+SO methods, respectively.

methods give very good agreement with each other with the MRCI splitting being 4–5 cm^{-1} lower in energy for all angles considered. The difference between the MRCI+SO calculation and the MRCI calculation is considerably larger, with differences between the two methods of 58–64 cm^{-1} , and the largest differences occurring at the equilibrium geometry.

The second internal rotation considered, the in-plane internal rotation of the hydroxyl moiety, gave much different results, particularly in the magnitude of the splitting (see Fig. 9). For all three methods the derivative of ΔE with respect to ψ is considerably larger than the derivative with respect to θ . For sufficiently small vibrations about the equilibrium geometry, the derivative approaches zero for all three methods, but for large-amplitude vibrations, the magnitude of the derivative increases to as large as 15 $\text{cm}^{-1}/\text{deg}$. Near the middle of the range explored ($\psi \approx 18^\circ$), the derivative is about $-10.4 \text{ cm}^{-1}/\text{deg}$. Although not immediately obvious on the scale of Fig. 9, the curves are not exactly symmetrical about $\psi=0$ since the calculations are done at the equilibrium value of θ , which is not equal to 180° .

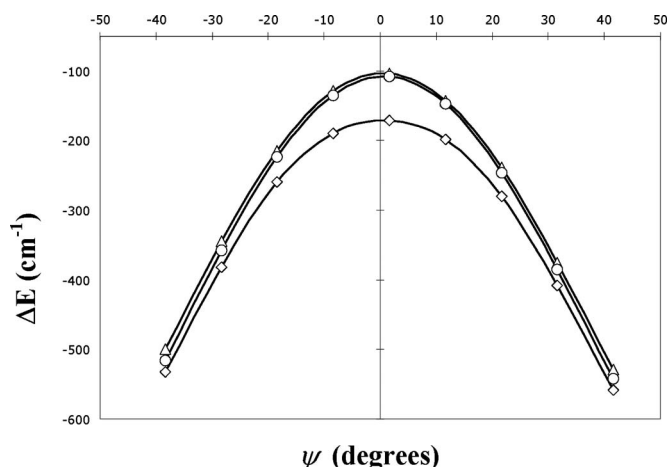


FIG. 9. Plot of $\Delta E \equiv E(^2A') - E(^2A'')$ (in cm^{-1}) vs ψ for rotation of OH radical about an axis parallel to the x -axis and through its center of mass (in-plane rotation). Triangles, circles, and diamonds indicate results obtained using the CASSCF, MRCI, and MRCI+SO methods, respectively.

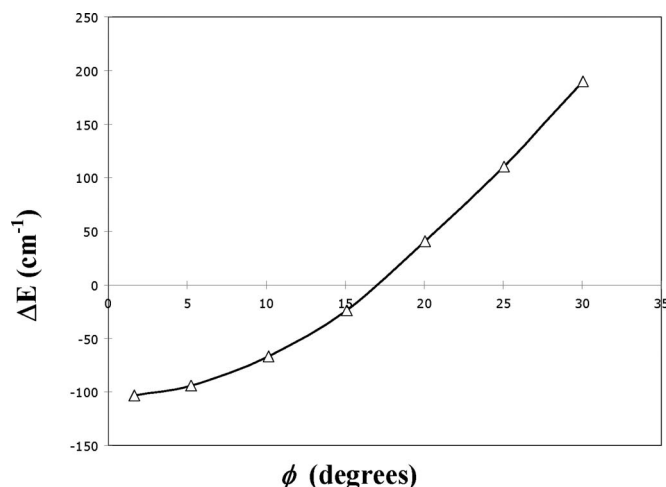


FIG. 10. Plot of $\Delta E \equiv E(^2A') - E(^2A'')$ (in cm^{-1}) vs ϕ for rotation of OH radical about an axis parallel to the y -axis and through its center of mass (out-of-plane rotation). Triangles indicate results obtained using the CASSCF method.

Out-of-plane vibration in the OH lowers the point group symmetry from C_s to C_1 . As a result, the number of configurations one must consider in both the MRCI and MRCI+SO calculation becomes very large and these calculations were not pursued. Figure 10 shows a plot of ΔE versus ϕ for the CASSCF calculation. Since the initial structure has C_s symmetry, the clockwise and counterclockwise internal rotations are the same, and thus internal rotation in only one direction was considered. In the C_1 symmetry there are no longer $^2A'$ and $^2A''$ states, but the energies of the wave functions corresponding to the same orbital occupations may be measured as a function of the angle of internal rotation. Figure 10 shows that near the equilibrium structure (the C_s structure) the derivative of ΔE with respect to ϕ again approaches zero, while at larger angles the derivative increases to as much as 16 $\text{cm}^{-1}/\text{deg}$. Near 18° , the derivative is about 13.5 $\text{cm}^{-1}/\text{deg}$. Figure 10 also shows that ΔE remains negative until an angle of approximately 17° , where a conical intersection is encountered in the absence of spin-orbit interaction. In a five-atom system, conical intersections occur in up to seven degrees of freedom. When spin-orbit interaction is added, a seven-dimensional seam of intersection is lowered to a four-dimensional one.⁶⁰

VI. DISCUSSION

The fitted values of ρ are in reasonable agreement between the isotopic forms studied, but the small isotopic dependence noted previously for the 16/16 and 18/18 species persists in this work. Moreover, while the magnitude of ρ increases by 0.040 57(13) cm^{-1} in $^{18}\text{OH}-^{18}\text{OH}_2$ relative to the parent species, the changes for the mixed isotopic forms are somewhat larger and in opposite directions. In particular, we observe that ^{18}O substitution on the OH decreases the magnitude of ρ by 0.068 64(11) cm^{-1} , while ^{18}O substitution on the water increases its magnitude by 0.105 29(10) cm^{-1} . The sum of these changes (accounting for their differences in sign) is 0.036 65(15) cm^{-1} and is of the order of the net effect observed for the 18/18 species.

Thus, the value of ρ obtained for $^{18}\text{OH}-^{18}\text{OH}_2$ arises, at least to a first approximation, from partial cancellation of larger, opposing changes upon single isotopic substitution.

The most obvious cause for the apparent changes in ρ is a genuine dependence of the state splitting on the relative orientation of OH and H₂O, with subtle changes in vibrationally averaged structure upon substitution producing the observed variation. The plausibility of such a scenario can be examined in the context of Figs. 8–10, which illustrate the variation in ΔE as a function of large-amplitude angular motion of the OH and water moieties. Considering, first, motion along the water inversion coordinate (θ in Figs. 4, 5, and 8), we observe that the magnitude of ΔE increases (i.e., ΔE becomes more negative) as the water approaches the planar configuration. To the extent that the small ($\sim 15\text{ cm}^{-1}$) barrier can be ignored, the H₂¹⁸O in the complex will be localized nearer to the planar configuration, yielding a more negative vibrationally averaged value of ΔE . Qualitatively, this is in agreement with the spectroscopic observations in which ρ decreases (becomes more negative) by $0.105\ 29(10)\text{ cm}^{-1}$. Note that if the barrier to inversion were significant relative to the zero point energy, ¹⁸O substitution would have the opposite effect of localizing the system at the nonplanar geometry, causing ρ to increase (i.e., become less negative). The present results, therefore, are consistent with a very low barrier.

That the magnitude of such an effect is reasonable can be seen from a crude calculation in which the reduction in vibrational amplitude upon isotopic substitution is estimated within the harmonic approximation, and the resulting effect on ρ is then estimated from the calculated derivatives with respect to angles. Since the inversion motion of water in the complex corresponds roughly to rotation about its *a*-inertial axis, the effective moment of inertia for this vibration may be approximated as the *A* rotational constant of H₂O. Invoking a harmonic approximation in the angle $\gamma \equiv (180^\circ - \theta)$, and recognizing that $\langle \gamma^2 \rangle^2$ scales inversely as the moment of inertia for the bend,⁵⁹ the value of $\gamma_{\text{rms}} \equiv \langle \gamma^2 \rangle^{1/2}$ scales roughly as $[A(\text{H}_2\text{O})]^{1/4}$. Using the *A* rotational constants for H₂¹⁶O (Ref. 61) and H₂¹⁸O (Ref. 62) gives $\gamma_{\text{rms}}(\text{H}_2^{16}\text{O})/\gamma_{\text{rms}}(\text{H}_2^{18}\text{O})=1.003$. The value of γ_{rms} itself is not known for either isotopic form, but if we estimate it to be near the equilibrium value of $\gamma=34^\circ$ (Fig. 3), this corresponds to a value of $d\gamma_{\text{rms}} \equiv \gamma_{\text{rms}}(\text{H}_2^{18}\text{O}) - \gamma_{\text{rms}}(\text{H}_2^{16}\text{O}) = -0.1^\circ$. Using the value of $d(\Delta E)/d\theta = -0.6\text{ cm}^{-1}/\text{deg}$ noted above, and accounting for the relationship $\Delta E = -(\rho^2 + A_{\text{SO}}^2)^{1/2}$, a value of $d\theta_{\text{rms}} = -d\gamma_{\text{rms}} = 0.1^\circ$ implies a value of $d\rho = -(d\Delta E/d\theta)(\rho^2 + A_{\text{SO}}^2)^{1/2}(1/\rho)d\theta_{\text{rms}} = -0.08\text{ cm}^{-1}$, which is in remarkable agreement with the observed value of -0.105 cm^{-1} . A more accurate calculation would, of course, require averaging ρ over vibrational wave functions corresponding to the inversion potential, a procedure that has not been performed. However, this simple calculation clearly gives the correct sign and magnitude for the observed change and, thus, indicates the plausibility of the vibrational averaging effect as the primary cause of the change in ρ upon ¹⁸O substitution on the water.

The effect of vibrational averaging of the OH moiety is more complex because $d(\Delta E)/d\psi$ and $d(\Delta E)/d\phi$ are of op-

posite signs and vary considerably more than $d(\Delta E)/d\theta$ over the range of relevant angles. Nonetheless, if the rms values of ψ and ϕ are scaled with the fourth root of the *B* rotational constants for ¹⁶OH (Ref. 40) and ¹⁸OH,⁴¹ and if their magnitudes are taken to be similar to the 18° value determined for HF in H₂O–HF,⁶³ a decrease of 0.03° upon ¹⁸O substitution is calculated. Although the *ab initio* calculations for ΔE performed along the ϕ coordinate were done only at the CASSCF level, it is likely (based on Figs. 8 and 9) that the derivatives of ρ with respect to these angles would be similar, had the calculations been repeated using the MRCI and MRCI+SO methods. Thus, using $d\psi=d\phi=-0.03^\circ$, together with values of $d(\Delta E)/d\psi=-10.4\text{ cm}^{-1}/\text{deg}$ and $d(\Delta E)/d\phi=13.5\text{ cm}^{-1}/\text{deg}$ from Figs. 9 and 10, respectively, an estimated value of $d\rho=+0.13\text{ cm}^{-1}$ is obtained. Once again, the calculation is quite crude but it compares sufficiently well in both sign and magnitude with the observed value of 0.069 cm^{-1} that it supports vibrational averaging as the main contribution to the isotopic changes in ρ .

VII. CONCLUSION

Spectroscopic observations of ¹⁶OH–¹⁶OH₂ and its ¹⁸O substituted forms reveal small ($<0.11\text{ cm}^{-1}$) differences in the fitted values of the quenching parameter ρ . Substitution on the H₂O moiety increases $|\rho|$, while that on the OH decreases it, and the small increase observed for the doubly substituted form (¹⁸OH–¹⁸OH₂) arises roughly from the net result of these two opposing changes. The fitted value of ρ for the parent species implies an energy separation of 203.76 cm^{-1} between the ground (²A') and first excited (²A'') states. A direct measurement of this energy, possibly by infrared combination differences, would provide a valuable test of the spectroscopic model employed. *Ab initio* calculations of this separation, performed with QCISD as well as MRCI, both with and without the inclusion of spin-orbit coupling have been performed. The MRCI calculations with spin-orbit coupling yield the best results, giving a value of ΔE within about 16% of the experimental value. Calculations of ΔE along the large-amplitude bending coordinates of the OH and OH₂ moieties are consistent with vibrational averaging as the main cause of the observed isotopic sensitivity of ρ .

ACKNOWLEDGMENTS

We are grateful to Professor Y. Endo and Dr. Y. Sumiyoshi for sharing their unpublished frequencies with us. This work was supported by the National Science Foundation (Grant Nos. CHE 0514256 and CHE 0517895), the donors of the Petroleum Research Fund administered by the American Chemical Society, the U.S. Department of Energy (Grant No. DE-FG02-86ER13579), and the Minnesota Supercomputing Institute.

¹ K. S. Kim, H. S. Kim, J. H. Jang, H. S. Kim, B.-J. Mhin, Y. Xie, and H. F. Schaefer III, *J. Chem. Phys.* **94**, 2057 (1991).

² Y. Xie and H. F. Schaefer III, *J. Chem. Phys.* **98**, 8829 (1993).

³ B. Wang, H. Hou, and Y. Gu, *Chem. Phys. Lett.* **303**, 96 (1999).

⁴ V. S. Langford, A. J. McKinley, and T. I. Quickenden, *J. Am. Chem. Soc.* **122**, 12859 (2000).

- ⁵Z. Zhou, Y. Qu, A. Fu, B. Du, F. He, and H. Gao, *Int. J. Quantum Chem.* **89**, 550 (2002).
- ⁶P. D. Cooper, H. G. Kjaergaard, V. S. Langford, A. J. McKinley, T. I. Quickenden, and D. P. Schofield, *J. Am. Chem. Soc.* **125**, 6048 (2003).
- ⁷A. Engdahl, G. Karlström, and B. Nelander, *J. Chem. Phys.* **118**, 7797 (2003).
- ⁸D. P. Schofield and H. G. Kjaergaard, *J. Chem. Phys.* **120**, 6930 (2004).
- ⁹M. D. Marshall and M. I. Lester, *J. Phys. Chem. B* **109**, 8400 (2005).
- ¹⁰C. S. Brauer, G. Sedo, E. M. Grumstrup, K. R. Leopold, M. D. Marshall, and H. O. Leung, *Chem. Phys. Lett.* **401**, 420 (2005).
- ¹¹Y. Ohshima, K. Sato, Y. Sumiyoshi, and Y. Endo, *J. Am. Chem. Soc.* **127**, 1108 (2005).
- ¹²X.-L. Dong, Z.-Y. Zhou, L.-J. Tian, and G. Zhao, *Int. J. Quantum Chem.* **102**, 461 (2005).
- ¹³T. D. Crawford, M. L. Abrams, R. A. King, J. R. Lane, D. P. Schofield, and H. G. Kjaergaard, *J. Chem. Phys.* **125**, 204302 (2006).
- ¹⁴M. A. Allodi, M. E. Dunn, J. Livada, K. N. Kirschner, and G. C. Shields, *J. Phys. Chem. A* **110**, 13283 (2006).
- ¹⁵S. Du, J. S. Francisco, G. K. Schenter, T. D. Iordanov, B. C. Garrett, M. Dupuis, and J. Li, *J. Chem. Phys.* **124**, 224318 (2006).
- ¹⁶D. C. McCabe, B. Rajakumar, P. Marshall, I. W. M. Smith, and A. R. Ravishankara, *Phys. Chem. Chem. Phys.* **8**, 4563 (2006).
- ¹⁷C.-H. Lai and P.-T. Chou, *J. Comput. Chem.* **28**, 1357 (2007).
- ¹⁸S. Aloisio and J. S. Francisco, *Acc. Chem. Res.* **33**, 825 (2000).
- ¹⁹V. Vaida, H. G. Kjaergaard, and K. Feierabend, *Int. Rev. Phys. Chem.* **22**, 203 (2003).
- ²⁰T. Uchimarui, A. K. Chandra, S. Tsuzuki, M. Sugie, and A. Sekiya, *J. Comput. Chem.* **24**, 1538 (2003).
- ²¹N. Karakus and R. Ozkan, *J. Mol. Struct.: THEOCHEM* **724**, 39 (2005).
- ²²B. A. Ellingson and D. G. Truhlar, *J. Am. Chem. Soc.* **129**, 12765 (2007).
- ²³P. Cabral do Couto, R. C. Guedes, B. J. Costa Cabral, and J. A. Martinho Simões, *J. Chem. Phys.* **119**, 7344 (2003).
- ²⁴P. Vassilev, M. J. Louwerse, and E. J. Baerends, *Chem. Phys. Lett.* **398**, 212 (2004).
- ²⁵J. M. Khalack and A. P. Lyubartsev, *J. Phys. Chem. A* **109**, 378 (2005).
- ²⁶(a) J. W. Bevan, Z. Kisiel, A. C. Legon, D. J. Millen, and S. C. Rogers, *Proc. R. Soc. London* **372**, 441 (1980); (b) Z. Kisiel, A. C. Legon, and D. J. Millen, *ibid.* **381**, 419 (1982).
- ²⁷M. D. Marshall and M. I. Lester, *J. Chem. Phys.* **121**, 3019 (2004).
- ²⁸J. B. Davey, M. E. Greenslade, M. D. Marshall, M. I. Lester, and M. D. Wheeler, *J. Chem. Phys.* **121**, 3009 (2004).
- ²⁹W. M. Fawzy and J. T. Hougen, *J. Mol. Spectrosc.* **137**, 154 (1989).
- ³⁰J. A. Phillips, M. Canagaratna, H. Goodfriend, A. Grushow, J. Almlöf, and K. R. Leopold, *J. Am. Chem. Soc.* **117**, 12549 (1995).
- ³¹We are grateful to Dr. Y. Sumiyoshi and Professor Y. Endo for bringing to our attention discrepancies between their observed frequencies and those of our previous work.
- ³²Subsequent to the replacement of our support rods, all of our newly measured frequencies for the parent species agreed with those of Ohshima *et al.* (Ref. 11) to within 22 kHz, with most agreeing to better than 10 kHz.
- ³³W. L. Meerts and A. Dymanus, *Can. J. Phys.* **53**, 2123 (1975).
- ³⁴Y. Ohshima, M. Iida, and Y. Endo, *J. Chem. Phys.* **95**, 7001 (1991).
- ³⁵Y. Kasai, K. Obi, Y. Ohshima, Y. Endo, and K. Kawaguchi, *J. Chem. Phys.* **103**, 90 (1995).
- ³⁶Y. Sumiyoshi, Y. Endo, and Y. Ohshima, *J. Chem. Phys.* **113**, 10121 (2000).
- ³⁷S. Wu and K.R. Leopold (unpublished).
- ³⁸P. D. A. Mills, C. M. Western, and B. J. Howard, *J. Phys. Chem.* **90**, 3331 (1986).
- ³⁹C. R. Dennis, C. J. Whitham, and B. J. Howard, *J. Chem. Phys.* **115**, 1367 (2001).
- ⁴⁰J. M. Brown, C. M. L. Kerr, F. D. Wayne, K. M. Evenson, and H. E. Radford, *J. Mol. Spectrosc.* **86**, 544 (1981).
- ⁴¹E. R. Comben, J. M. Brown, T. C. Steimle, K. R. Leopold, and K. M. Evenson, *Astrophys. J.* **305**, 513 (1986).
- ⁴²NIST Physical Reference Data: <http://physics.nist.gov/PhysRefData/MolSpec/Diatomic/Html/Tables/OH.html>.
- ⁴³Our previous work employed the values $A_{\text{SO}}(^{16}\text{OH}) = -4\,157\,663$ MHz and $A_{\text{SO}}(^{18}\text{OH}) = -4\,157\,071$ MHz. The current fits employ better values, $A_{\text{SO}}(^{16}\text{OH}) = -4\,168\,639.13$ MHz and $A_{\text{SO}}(^{18}\text{OH}) = -4\,168\,644.9$ MHz taken from Refs. 40 and 41.
- ⁴⁴S. Wu, G. Sedo, E. M. Grumstrup, and K. R. Leopold, *J. Chem. Phys.* **127**, 204315 (2007).
- ⁴⁵H. M. Pickett, *J. Mol. Spectrosc.* **148**, 371 (1991).
- ⁴⁶The energy interval referred to in Ref. 11 is the off-diagonal element of the 2×2 matrix described in that paper and thus corresponds exactly to our parameter, ρ . Y. Sumiyoshi, private communication (July 3, 2008).
- ⁴⁷J. A. Pople, M. Head-Gordon, and K. Raghavachari, *J. Chem. Phys.* **87**, 5968 (1987).
- ⁴⁸R. Krishnan, J. S. Binkley, R. Seeger, and J. A. Pople, *J. Chem. Phys.* **72**, 650 (1980).
- ⁴⁹T. Clark, J. Chandrasekhar, G. W. Spitznagel, and P. v. R. Schleyer, *J. Comput. Chem.* **4**, 294 (1983).
- ⁵⁰M. J. Frisch, J. A. Pople, and J. S. Binkley, *J. Chem. Phys.* **80**, 3265 (1984).
- ⁵¹M. J. Frisch, G. W. Trucks, H. B. Schlegel *et al.*, GAUSSIAN 03, Revision C.02, Gaussian, Inc., Wallingford, CT, 2004.
- ⁵²P. J. Knowles and H.-J. Werner, *Chem. Phys. Lett.* **145**, 514 (1988).
- ⁵³H.-J. Werner and P. J. Knowles, *J. Chem. Phys.* **89**, 5803 (1988).
- ⁵⁴H.-J. Werner and P. J. Knowles, *J. Chem. Phys.* **82**, 5053 (1985).
- ⁵⁵A. Berning, M. Schweizer, H.-J. Werner, P. J. Knowles, and P. Palmieri, *Mol. Phys.* **98**, 1823 (2000).
- ⁵⁶H.-J. Werner, P. J. Knowles, R. Lindh, M. Schuetz *et al.*, MOLPRO-version 2002.6, University of Birmingham, Birmingham, 2002, see <http://www.molpro.net>.
- ⁵⁷C. C. J. Roothaan, *Rev. Mod. Phys.* **32**, 179 (1960).
- ⁵⁸Z. Kisiel, A. C. Legon, and D. J. Millen, *J. Mol. Struct.* **112**, 1 (1984).
- ⁵⁹G. T. Fraser, F. J. Lovas, and R. D. Suenram, *J. Chem. Phys.* **84**, 5983 (1986).
- ⁶⁰C. A. Mead, *J. Chem. Phys.* **70**, 2276 (1979).
- ⁶¹F. C. De Lucia, P. Helminger, R. L. Cook, and W. Gordy, *Phys. Rev. A* **5**, 487 (1972).
- ⁶²F. C. De Lucia, P. Helminger, R. L. Cook, and W. Gordy, *Phys. Rev. A* **6**, 1324 (1972).
- ⁶³A. C. Legon and L. C. Willoughby, *Chem. Phys. Lett.* **92**, 333 (1982).